Low Mach number aeroacoustic computations of airfoils in application with Pierce's wave equation

Étienne Spieser, Xin Zhang

inter·noise 2023
CHIBA,GREATER TOKYO 20-23 AUGUST

Low Mach number aeroacoustic computations of airfoils in application with Pierce's wave equation

Étienne Spieser[1], Xin Zhang[2]
Department of Mechanical and Aerospace Engineering,
The Hong Kong University of Science and Technology,
Clear Water Bay, Kowloon, Hong Kong SAR, China

ABSTRACT

The airflows generated by drones are fairly different from those arising for conventional aeronautical architectures. They are low Mach number, relatively low Reynolds number and transient regimes play a dominant role. The goals of this work are twofold. This study firstly seeks to present an aeroacoustic model built on Pierce's wave equation, which is adapted to the specificity of this physic, and which is consistent and robust. The second part of this contribution then focuses on the use and the validation of a high-order highly scalable solver relying on an open source C++ library to solve the large scales of the flow turbulence by means of an explicit filtering. The flow corresponding to a benchmarked $Re = 5 \cdot 10^4$ *airfoil in full stall is computed and results are briefly discussed.*

1. INTRODUCTION

Acoustic analogies have originally been designed to model flow noise arising in aeronautical applications such as jets [1, 2], propellers or airframe systems [3]. In the context of these high Mach number flows, the proper separation between the noise generation and the sound propagation mechanisms, as well as the taking into account of the source motion, represented a challenging task, and has drawn a considerable attention back then in the emerging aeroacoustic community. Starting from the general set of fluid dynamics equations, these efforts have led to formulate different wave operators to separate the sound generation process from its propagation [4–7]. Yet, as illustrated by Goldstein [8, 9], the choice of the base flow about which the variables are decomposed is to a large extent independent of the selection of an acoustic analogy, and represents another decisive parameter in the design of an acoustic analogy that is suited to the physics studied. In the above-mentioned formulations, the mean flow is taken as the base flow, and the acoustic fluctuations are solutions of a Reynolds decomposition of the flow variables. Sound sources are then generally modelled from non-linear second-order perturbations and have to be informed either numerically [7] or from ad-hoc theoretical models [10]. While this approach can handle any flow Mach number, this strategy fails to satisfactorily model transient phenomena, such as those encountered in the case of large-scale upstream flow disturbances or in the case of a change of trajectory of a drone.

Acoustic analogies constructed as an Expansion about an Incompressible Flow (EIF) overcome this difficulty by taking the solution of the unsteady incompressible Navier-Stokes equations as the base flow. The idea of EIF has initially been introduced by Ribner [11] as an attempt to present an alternative to Lighthill's theory that is built on more intuitive sound sources. In this scope, sound

[1] meetiennes@ust.hk

[2] aexzhang@ust.hk

sources are directly modelled from the incompressible base flow, while the acoustic fluctuations are sought as the compressible deviation from this solenoidal base flow. Since Ribner's dilatation theory, this approach has received additional theoretical justification by Klainerman and Majda [12] and was implemented and validated by Hardin and Pope [13]. Notable contributions using this method have then been made by Shen and Sørensen [14–16] Seo and Moon [17, 18] and others [19–21].

In this study, an EIF for Pierce's wave equation [22] is presented to generalise Ribner's dilatation theory to include sound propagation effects. This wave operator is selected as it is unconditionally stable due to its energy conservation property [23], fairly accurate [24, 25] and numerically less expensive than the complete set of linearised Euler's equations. An acoustic analogy based on Pierce's wave equation, that relies on a Reynolds decomposition of the flow, has recently been used to compute the sound radiated by a mixing layer [26]. In this previous investigation, the sound source was obtained from the spatial filtering of Lighthill's stress tensor. The alternative formulation based on Ribner's idea provides a framework more suited to the study of transient phenomena and, at the same time, simplifies the tracking of the sound source.

In what follows, this acoustic analogy based on an EIF tailored to Pierce's equation is detailed and compared to Ribner's dilatation theory. The remaining part of this proceeding then focuses on the numerical modelling of the large scales of the base flow that contains the sound sources, using an efficient high-order incompressible flow solver based on the finite element methods library MFEM.

2. LOW MACH NUMBER ACOUSTIC ANALOGY

To compute the noise radiated by low Mach number transient flows and identify the sources of sound, solutions of incompressible Navier-Stokes equations are considered to define the base flow of the acoustic analogy presented here. The dynamics of incompressible flows is governed by the incompressible velocity $\mathbf{u}_0$ and the pseudosound p_0, and verifies,

$$\begin{cases} \nabla \cdot \mathbf{u}_0 = 0 \\ \dfrac{\mathrm{D}\mathbf{u}_0}{\mathrm{D}t} - \nu \Delta \mathbf{u}_0 + \nabla \left(\dfrac{p_0}{\rho_0} \right) = \mathbf{0} \end{cases} \tag{1}$$

where $\mathrm{D}/\mathrm{D}t = \partial/\partial t + \mathbf{u}_0 \cdot \nabla$ is the material derivative, ρ_0 is the constant density and ν is the kinematic viscosity. In the framework of expansions about incompressible flows, the acoustic solution is expressed as the fluctuations superposed to the base flow, that fulfils compressible Navier-Stokes equations. That is, if $\mathbf{u}$ and p are the velocity and pressure fields that verify compressible Navier-Stokes equations, the acoustic velocity $\mathbf{u}'$ and pressure p' verify $\mathbf{u} = \mathbf{u}_0 + \mathbf{u}'$ and $p = p_0 + p'$. The set of incompressible Navier-Stokes equations (1) is composed of the continuity and the momentum equations. To derive the acoustic model, the energy equation written for a perfect gas is considered. Applying an EIF to this equation and neglecting second-order interaction terms yield,

$$\frac{\mathrm{D}p'}{\mathrm{D}t} + \gamma p_0 (\nabla \cdot \mathbf{u}') + \mathbf{u}' \cdot \nabla p_0 = -\frac{\mathrm{D}p_0}{\mathrm{D}t} \tag{2}$$

Introducing the acoustic potential as $p' = -\mathrm{D}\phi/\mathrm{D}t$ and $\rho_0 \mathbf{u}' = \nabla \phi$, leads to the formula,

$$\frac{\mathrm{D}^2 \phi}{\mathrm{D}t^2} - \nabla \cdot (a_0^2 \nabla \phi) + \frac{\gamma - 1}{\gamma} \nabla \left(a_0^2 \right) \cdot \nabla \phi = \frac{\mathrm{D}p_0}{\mathrm{D}t} \tag{3}$$

where $a_0^2 = \gamma p_0 / \rho_0$ is the formal expression of the speed of sound for a perfect gas. It should be stated that this speed of sound is constructed from the incompressible flow field, for which ρ_0 is kept constant and may arbitrarily be defined. Thus, gradients of a_0 only account for the gradients in the pseudosound p_0 which effects on the propagation of sound is in many applications of lesser important

than variations of the mean density ρ_0, as obtained for example in the case of temperature gradients of the media [25]. This has to be seen as an intrinsic limitation to acoustic analogies based on EIF approaches. Because the physical relevance of the third term on the left-hand side of equation (3) is debatable, that it vanishes in the acoustic high frequency limit, and in order to retrieve Pierce's wave operator for which several interesting properties on the energy can be derived [23], this third term is discarded.

The expansion about incompressible flow (EIF) for Pierce's wave equation thus reads,

$$\frac{\mathrm{D}^2\phi}{\mathrm{D}t^2} - \nabla\cdot(a_0^2\nabla\phi) = \frac{\mathrm{D}p_0}{\mathrm{D}t} \qquad \text{with} \qquad p' = -\frac{\mathrm{D}\phi}{\mathrm{D}t} \tag{4}$$

This acoustic model can be viewed as an extension to Ribner's dilatation theory of the 60s [11],

$$\frac{\partial^2 p'}{\partial t^2} - a_0^2\Delta p' = -\frac{\partial^2 p_0}{\partial t^2} \tag{5}$$

The similarity of the two models is manifest, and in configurations where the flow velocity can be neglected, both models trivially coincide. The main differences lie in the ability of the proposed formulation to describe the effects of sound propagation and in the order of derivation of the sound source. The acoustic analogy proposed in equation (4) is an alternative to the one presented in [26], that is suited to model the aeroacoustic of transient flow regimes, but which is a priori restricted to low Mach number flows.

3. NUMERICAL FRAMEWORK

In the following, a methodology to calculate the incompressible base flow and the sound sources of the acoustic analogy previously presented is detailed. To be able to model complex geometries and to perform high-order calculations, a Finite Element Method (FEM) environment is chosen. To enable future developments, an open source environment is selected.

3.1. Flow modelling

The implementation of the incompressible Navier-Stokes equations by Franco *et al.* [27] based on the finite element library MFEM [28] developed at Lawrence Livermore National Laboratory (LLNL) is chosen for this work. The methodology to solve the set of equation (1) is implemented using high-order finite element discretization in space, and a third order implicit-explicit method in time which leverages an extrapolation scheme for the convective parts and a backward-difference formulation for the viscous parts of the equation. An implementation of the spatial filter of Fischer and Mullen [29] is used to stabilise the calculation of turbulent flows and filter out the scales of the flow that cannot be resolved by the grid size and order of the elements considered. A similar technique is used by Bogey and Bailly [30] to perform Large Eddy Simulation (LES) of jets without subgrid model. While this highly scalable solver supports GPU acceleration [27], parallel calculations are performed using only the MPI protocol. Numerical truncation of the computational domain is achieved using a buffer zone in which a spring force is applied in the momentum equation to gradually restore $\mathbf{u}_0$ to the ambient condition. The outer boundaries are then simply enforced with Dirichlet boundary conditions.

3.2. Benchmark problem

The Reynolds number for commercial micro air vehicle typically ranges between 10^4 and $5\cdot10^5$. To test the ability of the incompressible Navier-Stokes solver chosen to correctly describe the flow fields at these Reynolds numbers, the flow past a NACA 0012 airfoil with 12-degree angle of attack at a Reynolds number of $5\cdot10^4$ is studied. This configuration has previously been

benchmarked by Rodriguez *et al.* [31, 32] using Direct Numerical Simulation (DNS) resolution of the incompressible Navier-Stokes equations, their computation serves as a reference for the present study and for additional validations not presented here. At this angle of attack and Reynolds number, the airfoil is in full stall but is not far from the attached boundary layer configuration, making it a challenging case to reproduce.

3.3. Meshing

The NACA 0012 geometry with blunt trailing edge is meshed using the open source mesh generator Gmsh [33]. A customisable script to create partially structured grids of hexahedral elements is created[3]. The grid used in this study is shown in figure 1 and possesses 3.34 million hexahedral elements. The cell height varies between $2.8 \cdot 10^{-3}c$ and $0.13\,c$, where c stands for the airfoil chord, and, the mesh is $0.2 \cdot c$ periodic in the spanwise direction as in [31]. The grid is extruded spanwise, so that the size of the grid spanwise is equal to the size of the grid chordwise for the skin elements of the profile.

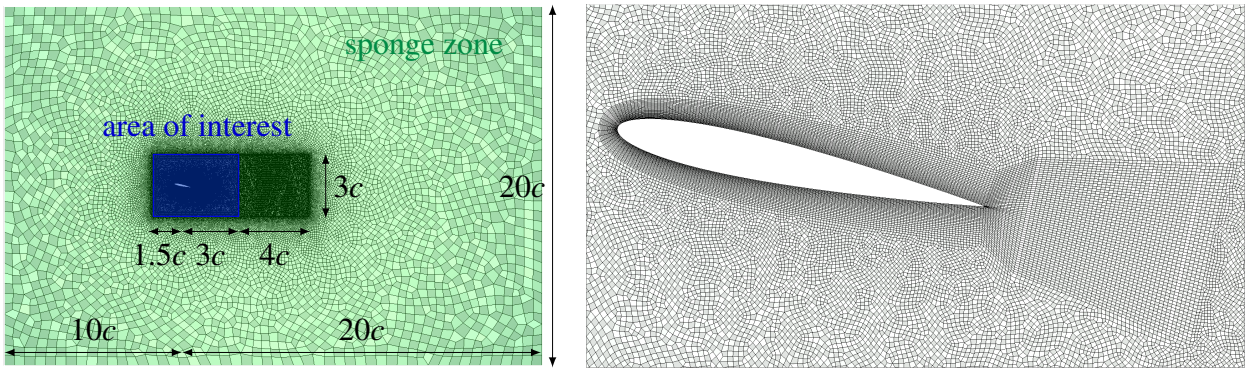

Figure 1: Extent of the total computation domain (left), and close-up of the structured boundary layer - wake region (right).

The quality of the grid presented here seems fairly satisfactory for this preliminary study. However, for now, it is a low order mesh and thus does not enable to benefit from the full efficiency of FEM. The mesh used, and shown in figure 1, presents 135 elements along the airfoil chord that are roughly equispaced. This is necessary to correctly capture the leading edge curvature, but prevents the use of high-order elements because of the prohibitive computational costs that would be associated with them. A perspective to this work is to adapt the mesh generation tool to high order elements.

3.4. Results

Two simulations are carried out with the mesh presented above, one with first order finite elements, the other with second order elements. They correspond respectively to 3.76 millions and 30.3 millions DOF for the pseudosound field p_0. 240 cores and 1200 cores have been used respectively for these computations on Tianhe2 cluster of the National Supercomputer Center of Guangzhou.

Figure 2 shows snapshots at two different times of the norm of the velocity field for the simulation run with second order elements. The instantaneous fields are taken at $t\,u_\infty/c = 9.54$ and $t\,u_\infty/c = 12.92$ to present two regimes of the flow around the airfoil. Here, u_∞ corresponds to the norm of the ambient, undisturbed velocity field. For the first time shown, the boundary layer is turbulent and attached to the airfoil. The second snapshot is chosen at the instant the airfoil starts to stall, from that moment on, a periodic vortex shedding is triggered, see [31, fig. 7]. For the simulation

[3] see the script `gmshRodAirfoil.py` available at https://github.com/etiennespieser/Propeller_Gmsh.

computed on the mesh with order 1 elements, not shown here for brevity, the airfoil does not stall. Even after a long time of simulation, the turbulent boundary layer remains attached in the simulation considering order 1 elements. When focusing on the flow around the leading edge of the airfoil for this lowest order simulation, grid to grid oscillations are visible, suggesting the solution is mesh dependant and the flow physics is not well captured at the precise location where the boundary layer separation is expected to occur. This aside, the computation with order 1 elements is stable and the computed flow field strongly resembles to the one obtained with order 2 elements before the stall.

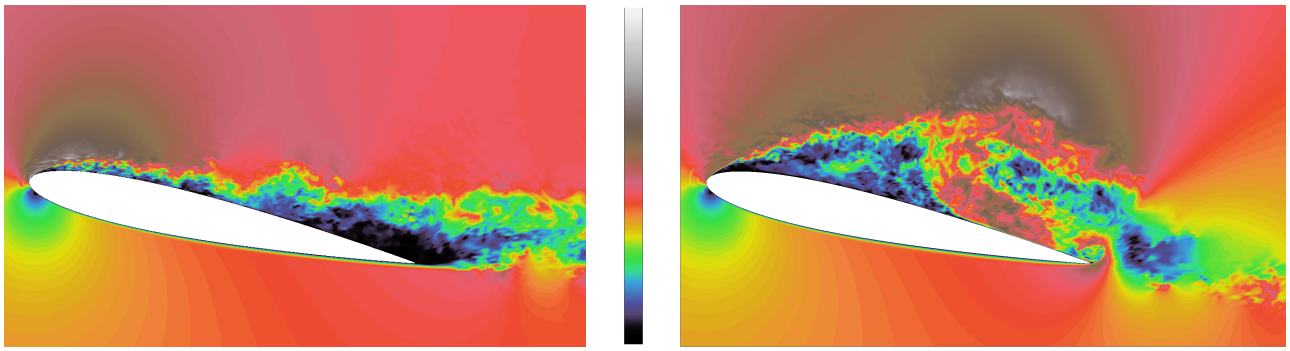

Figure 2: Instant velocity magnitude at $t\,u_\infty/c = 9.54$ (left) and $t\,u_\infty/c = 12.92$ (right) for the grid with order 2 elements, where $|\mathbf{u}_0|/u_\infty \in [0, 2.37]$.

To provide a more quantitative description of this transition, the time signals of the streamwise velocity field $u_{0,1}$ are compared for the two simulations at a given probe location. Figure 3 shows the normalised streamwise velocity fluctuations for the probe P5 located at $(0.693c, 0.106c)$, where the coordinate system is centred at the profile half cord, and where the axis are oriented along the flow and along the flow transverse directions. Probe P5 is located downstream of the trailing edge, slightly above the chord line, see [31, fig. 5] for more details on the probe location. The transition for the finer simulation is clearly visible in the time signal of the velocity. Around $t\,u_\infty/c = 13$, the signal suddenly changes from a high frequency, low amplitude stochastic process to a high amplitude low frequency periodic signal, compare also with [31, fig. 9(b)]. These periodic patterns are not visible in the signal corresponding to the simulation done with elements of order 1, even for longer times.

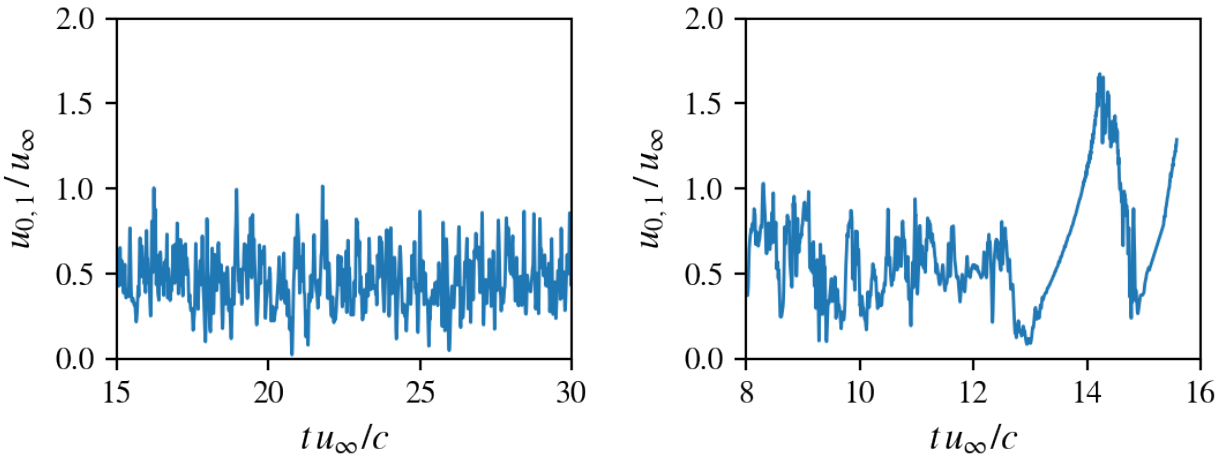

Figure 3: Time signal of the normalised streamwise velocity fluctuations at the probe P5. Results obtained with finite elements of order 1 (left) and with elements of order 2 (right).

The probe P5 is located in the turbulent wake of the airfoil. Comparing the statistics of the lowest order simulation with those of the higher order one can provide indication on properties of the

spatial filter implemented. As an opening for further validation that will follow, figure 4 compares the power spectral densities of these streamwise velocities for both simulations considering times for which the turbulent boundary layers are attached, and hence for which the flows are comparable. The signals are not satisfactorily converged yet, however a turning point at $f\,c/u_\infty = 20$ is clearly visible. Before this frequency, signals fairly agree, after the power spectral density associated with the coarser simulations tumbles. This frequency is the cut-off frequency imposed by the mesh, the order of the finite elements and the filter considered.

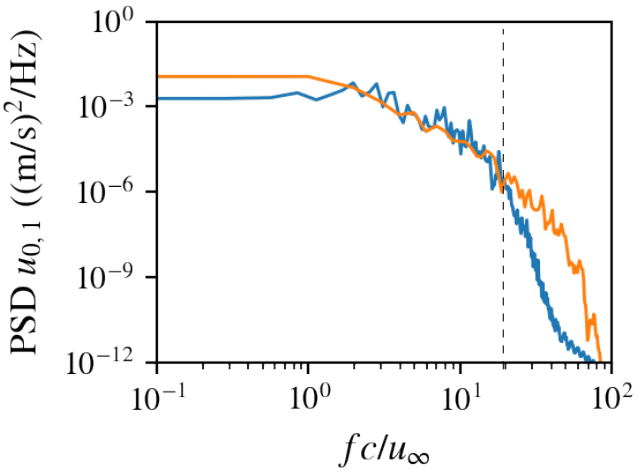

Figure 4: Power spectral density of the streamwise velocity fluctuation in the wake of the attached boundary layer, computed with order 1 finite elements (blue) and with order 2 elements (orange).

4. CONCLUSION

Low Mach number acoustic analogies were historically created to make problems analytically tractable, and to provide insight into the mechanisms of sound generation. In the era of computational aeroacoustics, these low Mach number formulations can be used to solve transient problems for which conventional acoustic analogies are not suitable. This study presented a modern reformulation of Ribner's dilation theory that is written for Pierce's wave equation. As a preliminary step to the implementation of this methodology, a numerical framework for accurately solving the base flow using advanced open source libraries is presented.

ACKNOWLEDGEMENTS

The authors would like to thank Zhong Siyang for the encouragement they benifited from, and the MFEM development team for making their tool available and user-friendly (www.mfem.org). The first author has received founding from the Hong Kong Innovation and Technology Commission (ITC): ITS/301/20FP and the Hong Kong Research Grants Council: 16204721. The authors also acknowledge National Supercomputing Center in Guangzhou Nansha Sub-center for providing access to the high-performance computational resources of Tianhe2.

REFERENCES

1. M. J. Lighthill, "The bakerian lecture, 1961 Sound generated aerodynamically," *Proceedings of the Royal Society of London. Series A. Mathematical and Physical Sciences*, vol. 267, no. 1329, pp. 147–182, 1962.
2. J. E. Ffowcs Williams, "The noise from turbulence convected at high speed," *Philosophical Transactions of the Royal Society A*, vol. 255, no. 1061, pp. 469–503, 1963.

3. M. E. Goldstein, *Aeroacoustics*. New York, McGraw-Hill International Book Co., 1976.
4. J. E. Ffowcs Williams and D. L. Hawkings, "Sound generation by turbulence and surfaces in arbitrary motion," *Proceedings of the Royal Society of London. Series A. Mathematical and Physical Sciences*, vol. 264, no. 1151, pp. 321–342, 1969.
5. O. M. Phillips, "On the generation of sound by supersonic turbulent shear layers," *Journal of Fluid Mechanics*, vol. 9, no. 1, pp. 1–28, 1960.
6. G. M. Lilley, H. E. Plumblee, W. C. Strahle, S. Y. Ruo, and P. E. Doak, "The generation and radiation of supersonic jet noise. Volume IV. Theory of turbulence generated jet noise, noise radiation from upstream sources, and combustion noise.," tech. rep., Lockheed-Georgia Co. Marietta, 1972.
7. C. Bogey, C. Bailly, and D. Juvé, "Computation of flow noise using source terms in linearized Euler's equations," *AIAA Journal*, vol. 40, no. 2, pp. 235–243, 2002.
8. M. E. Goldstein, "A generalized acoustic analogy," *Journal of Fluid Mechanics*, vol. 488, pp. 315–333, 2003.
9. M. E. Goldstein, "On identifying the true sources of aerodynamic sound," *Journal of Fluid Mechanics*, vol. 526, p. 337, 2005.
10. M. Z. Afsar, "Insight into the two-source structure of the jet noise spectrum using a generalized shell model of turbulence," *European Journal of Mechanics-B/Fluids*, vol. 31, pp. 129–139, 2012.
11. H. S. Ribner, "Aerodynamic sound from fluid dilitations. A theory of the sound from jets and other flows," tech. rep., University of Toronto, Institute of aerophysics, 1962. UTIA Report N^o 86, AFOSR TN 3430.
12. S. Klainerman and A. Majda, "Compressible and incompressible fluids," *Communications on Pure and Applied Mathematics*, vol. 35, pp. 629–651, 1982.
13. J. C. Hardin and D. S. Pope, "An acoustic/viscous splitting technique for computational aeroacoustics," *Theoretical and computational fluid dynamics*, vol. 6, no. 5-6, pp. 323–340, 1994.
14. W. Z. Shen and J. N. Sørensen, "Comment on the aeroacoustic formulation of Hardin and Pope," *AIAA Journal*, vol. 37, no. 1, pp. 141–143, 1999.
15. W. Z. Shen and J. N. Sørensen, "Aeroacoustic modeling of turbulent airfoil flows," *AIAA journal*, vol. 39, no. 6, pp. 1057–1064, 2001.
16. W. Z. Shen, W. Zhu, and J. N. Sørensen, "Aeroacoustic computations for turbulent airfoil flows," *AIAA journal*, vol. 47, no. 6, pp. 1518–1527, 2009.
17. J. H. Seo and Y. J. Moon, "Linearized perturbed compressible equations for low mach number aeroacoustics," *Journal of Computational Physics*, vol. 218, no. 2, pp. 702–719, 2006.
18. Y. J. Moon, J. H. Seo, Y. M. Bae, M. Roger, and S. Becker, "A hybrid prediction method for low-subsonic turbulent flow noise," *Computers & Fluids*, vol. 39, no. 7, pp. 1125–1135, 2010.
19. S. A. Slimon, M. C. Soteriou, and D. W. Davis, "Development of computational aeroacoustics equations for subsonic flows using a Mach number expansion approach," *Journal of Computational Physics*, vol. 159, no. 2, pp. 377–406, 2000.
20. C.-D. Munz, M. Dumbser, and S. Roller, "Linearized acoustic perturbation equations for low Mach number flow with variable density and temperature," *Journal of Computational Physics*, vol. 224, no. 1, pp. 352–364, 2007.
21. M. Kaltenbacher, A. Hüppe, A. Reppenhagen, M. Tautz, S. Becker, and W. Kuehnel, "Computational aeroacoustics for HVAC systems utilizing a hybrid approach," *SAE International Journal of Passenger Cars-Mechanical Systems*, vol. 9, no. 2016-01-1808, pp. 1047–1052, 2016.
22. A. D. Pierce, "Wave equation for sound in fluids with unsteady inhomogeneous flow," *The Journal of the Acoustical Society of America*, vol. 87, no. 6, pp. 2292–2299, 1990.

23. É. Spieser and C. Bailly, "L'équation de Pierce et ses lois de conservation," in *25ème Congrès Français de Mécanique (CFM)*, 2022.
24. É. Spieser and C. Bailly, "Sound propagation using an adjoint-based method," *Journal of Fluid Mechanics*, vol. 900, p. A5, 2020.
25. S. Le Bras, G. Gabard, and H. Bériot, "Direct and adjoint problems for sound propagation in non-uniform flows with lined and vibrating surfaces," *Journal of Fluid Mechanics*, vol. 953, p. A16, 2022.
26. S. Schoder, E. Spieser, H. Vincent, C. Bogey, and C. Bailly, "Acoustic modeling using the aeroacoustic wave equation based on Pierce's operator," *AIAA Journal*, vol. (to appear), 2023.
27. M. Franco, J.-S. Camier, J. Andrej, and W. Pazner, "High-order matrix-free incompressible flow solvers with GPU acceleration and low-order refined preconditioners," *Computers & Fluids*, vol. 203, p. 104541, 2020.
28. R. Anderson, J. Andrej, A. Barker, J. Bramwell, J.-S. Camier, J. Cerveny, V. Dobrev, Y. Dudouit, A. Fisher, T. Kolev, W. Pazner, M. Stowell, V. Tomov, I. Akkerman, J. Dahm, D. Medina, and S. Zampini, "MFEM: A modular finite element methods library," *Computers & Mathematics with Applications*, vol. 81, pp. 42–74, 2021.
29. P. Fischer and J. Mullen, "Filter-based stabilization of spectral element methods," *Comptes Rendus de l'Académie des Sciences-Series I - Mathematics*, vol. 332, no. 3, pp. 265–270, 2001.
30. C. Bogey and C. Bailly, "Computation of a high Reynolds number jet and its radiated noise using large eddy simulation based on explicit filtering," *Computers & fluids*, vol. 35, no. 10, pp. 1344–1358, 2006.
31. I. Rodríguez, O. Lehmkuhl, R. Borrell, and A. Oliva, "Direct numerical simulation of a NACA0012 in full stall," *International journal of heat and fluid flow*, vol. 43, pp. 194–203, 2013.
32. O. Lehmkuhl, I. Rodríguez, A. Baez, A. Oliva, and C. D. Pérez-Segarra, "On the large-eddy simulations for the flow around aerodynamic profiles using unstructured grids," *Computers & Fluids*, vol. 84, pp. 176–189, 2013.
33. C. Geuzaine and J.-F. Remacle, "Gmsh: A 3-D finite element mesh generator with built-in pre-and post-processing facilities," *International journal for numerical methods in engineering*, vol. 79, no. 11, pp. 1309–1331, 2009.